Cerebral Cortex, July 2019; 2844–2858

doi: 10.1093/cercor/bhy150
Advance Access Publication Date: 23 August 2018
Original Article

ORIGINAL ARTICLE

Functional Subdivisions of Magnocellular Cell Groups in Human Basal Forebrain: Test–Retest Resting-State Study at Ultra-high Field, and Meta-analysis

Rui Yuan[1], Bharat B. Biswal [1,3] and Laszlo Zaborszky[2]

[1]Department of Biomedical Engineering, New Jersey Institute of Technology, Newark, NJ 07102, USA, [2]Center for Molecular and Behavioral Neuroscience, Rutgers, The State University of New Jersey, Newark, NJ 07102, USA and [3]The Clinical Hospital of Chengdu Brain Science Institute, MOE Key Lab for Neuroinformation, University of Electronic Science and Technology of China, Chengdu 610054, PR China

Address correspondence to Bharat B. Biswal, Email: bbiswal@gmail.com or laszloz@newark.rutgers.edu orcid.org/0000-0002-3710-3500

Abstract

The heterogeneous neuronal subgroups of the basal forebrain corticopetal system (BFcs) have been shown to modulate cortical functions through their cholinergic, gamma-aminobutyric acid-ergic, and glutamatergic projections to the entire cortex. Although previous studies suggested that the basalo-cortical projection system influences various cognitive functions, particularly via its cholinergic component, these studies only focused on certain parts of the BFcs or nearby structures, leaving aside a more systematic picture of the functional connectivity of BFcs subcompartments. Moreover, these studies lacked the high-spatial resolution and the probability maps needed to identify specific subcompartments. Recent advances in the ultra-high field 7T functional magnetic resonance imaging (fMRI) provided potentially unprecedented spatial resolution of functional MRI images to study the subdivision of the BFcs. In this study, the BF space containing corticopetal cells was divided into 3 functionally distinct subdivisions based on functional connection to cortical regions derived from fMRI. The overall functional connection of each BFcs subdivision was examined with a test-retest study. Finally, a meta-analysis was used to study the related functional topics of each BF subdivision. Our results demonstrate distinct functional connectivity patterns of these subdivisions along the rostrocaudal axis of the BF. All three compartments have shown consistent segregation and overlap at specific target regions including the hippocampus, insula, thalamus, and the cingulate gyrus, suggesting functional integration and separation in BFcs.

Key words: 7-Tesla, basal forebrain, BOLD, fMRI, resting-state

Introduction

The basal forebrain (BF) is located close to the medial and ventral surfaces of the cerebral hemispheres, and contains several interlocked anatomical structures, including the basal nucleus of Meynert (BNM), the nucleus accumbens or ventral striatum, and cell groups underneath the globus pallidus bridging the centromedial amygdala to the bed nucleus of the stria terminalis (also named "extended amygdala"). The primate BNM comprises a set of large hyperchromic neurons, also referred as magnocellular neurons, which provide the major cholinergic innervation to the cerebral cortex (Mesulam et al. 1983; Hedreen et al. 1984; Saper and Chelimsky 1984; Mesulam and Geula 1988). The majority of these cholinergic magnocellular neurons project topographically to large and discrete cortical regions, such as frontal, cingulate, and temporal cortices (Jones et al. 1976; Bigl et al. 1982; Pearson et al. 1983; Bloem et al. 2014; Zaborszky et al. 2015). Anatomical studies in rodents and primates have shown that gamma-aminobutyric acid-ergic

(GABAergic) and glutamatergic corticopetal neurons as well as various peptidergic interneurons intermingle with the cholinergic neurons (Mesulam and Van Hoesen 1976; Smiley et al. 1999; Hur et al. 2009; Zaborszky et al. 2012, 2015) and modulate cortical functions in a complex fashion (Detari 2000; Zaborszky and Duque 2003; Lee et al. 2005).

The BF is highly involved in several cognitive functions, including attention, learning, memory, reward, and is also involved in basic neurobiological processes, such as arousal, sleep-wake control as well as cortical plasticity (Wilson and Rolls 1990; Richardson and DeLong 1991; Voytko et al. 1994; Chiba et al. 1995; Everitt and Robbins 1997; Kilgard and Merzenich 1998; Baxter and Chiba 1999; McGaughy et al. 2002; Conner et al. 2005; Sarter et al. 2006; Weinberger 2007; Xu et al. 2015). BF dysfunction has been associated with several neurodegenerative diseases, such as Alzheimer's (Price et al. 1986; Zaborszky et al. 2008), Parkinson's disease (PD; Candy et al. 1983; Whitehouse et al. 1983), Korsakoff's disease (Arendt et al. 1995), Down syndrome (Sweeney et al. 1989; Granholm et al. 2000), and psychotic disorders such as schizophrenia (Heimer 2000). Despite its broad involvement in cortical modulation, the details of the functional organization of the BF are not well understood.

Mesulam et al. (1983) contributed to the study of BF organization by introducing a Ch nomenclature that delineates cholinergic neurons based on their topography in the BF and their cortical targets in rodents and primates. However, it is difficult to consistently define subcompartments using this original Ch nomenclature because it lacks specific topographical landmarks in standardized MRI space. To address this issue, Zaborszky and colleagues developed stereotaxic probabilistic maps of the magnocellular BF space by delineating the various BF compartments on 2D images of silver-stained histological sections obtained from brains that were processed for postmortem T1-weighted MRI scanning. (Zaborszky et al. 2008). The simple subdivisions are reproducible and have been validated in several studies (Butler et al. 2013, 2014, 2018; Li et al. 2014; Kline et al. 2016; Lammers et al. 2016; Cantero et al. 2017; Zhang et al. 2017). Since the postmortem probabilistic maps were constructed primarily based on the presence of large neurons that are mostly cholinergic (see discussion in Zaborszky et al. (2008)), the BF space considered in this study is also called BF cholinergic space.

Resting-state functional MRI has been widely used to address the functional connectivity of brain regions in vivo (Biswal et al. 1995, 2010; Fox and Raichle 2007). Previous studies have used resting-state functional magnetic resonance imaging (fMRI) to characterize functional connectivity of major subcortical regions, such as the thalamus (Zhang et al. 2008; Yuan et al. 2016), the basal ganglia (Draganski et al. 2008; Choi et al. 2012), the amygdala (Roy et al. 2009), the cerebellum (Buckner et al. 2011), as well as the brain stem (Beissner et al. 2014). Previous studies also investigated resting-state functional connection (RSFC) of 2 neighboring structures, such as the nucleus accumbens (Cauda et al. 2011), and the bed nucleus of the stria terminalis (Torrisi et al. 2015), as well as the BNM (Li et al. 2014). However, limited spatial resolution, except the one by Torrisi et al. (2015) and absence of a probability map prevented most of these studies from identifying microstructural details, and a systematic accounting of the functional connectivity of the subdivisions of the BF corticopetal space (BFcs) remains to be investigated.

In the present study, we tested whether BF topographical (Mesulam et al., 1983; Zaborszky et al., 2008) or microstructural compartments (Zaborszky et al., 2008) correspond to functional networks or functional topics as defined in the literature. Utilizing high-resolution 7T functional MRI, we parceled the entire BFcs as delineated by the postmortem MRI (Zaborszky et al. 2008) into distinct subdivisions based on RSFC. This data-driven approach results in 3 compartments (clusters). Next, we investigated the test-retest RSFC patterns in each of these functional compartments. The relations between the functional connection of each compartment and major networks were explored. Furthermore, to have a comprehensive view of the BFcs system, we utilized meta-analysis based on task responses in order to explore co-activation maps of each compartment and its related cognitive processes. Our results demonstrate distinct functional connectivity patterns and functional topics of these 3 clusters along the rostrocaudal axis of the BF.

Materials and Methods

Data Acquisition

High-resolution 7-Tesla test-retest resting-state fMRI images and anatomical images were downloaded from the Max Planck research group (https://github.com/INCF/BIDS-examples/tree/master/7t_trt) (Gorgolewski et al. 2015), consisting of 21 subjects with 10 males and 11 females, aged from 18 to 26. The fMRI images were collected with 1.5 mm^3 isotropic voxel size, TR = 3 s, TE = 17 ms, FA = 70, FOV = 192*192 mm^2, 70 slices, and 300 time points. In total, each subject was scanned with 2 runs with 2 sessions. The second scan session occurred after 1 week of the first session. Considering the scanning design, we only used the first run of resting-state fMRI from each session. The first five-time points of resting-state data were removed, leaving 295-time frames for each subject. The T1-weighted anatomical scan was a magnetization-prepared rapid-acquisition gradient echo for each subject (MP2RAGE, 200 slices with a 320*320*240 matrix; voxel size 0.7 mm^3, TR = 5 s, TE = 2.45 ms).

Data Preprocessing

All functional MRI data were prepared by using SPM12 software package (http://www.fil.ion.ucl.ac.uk/spm/software/spm12/), AFNI (http://afni.nimh.nih.gov/afni/), as well as in-house programs in MATLAB (MathWorks). Functional MRI data were corrected for physiological motion effects (1) (respiratory and cardiac recordings resampled at 40 Hz) in time series by 3 dretroicor from AFNI; (2) corrected for field mapping to alleviate the spatial distortion; (3) aligned to correct for head motion, and co-registered with each subject's T1-weighted images; (4) 6 motion parameters, obtained by rigid body registration and squared motion parameters, motion derivatives, motion forward derivatives and 13 slice-based regressors generated from physiological recordings (using RetroTS.m) have been regressed out; (5) the subject's structural images were segmented into grey matter (GM), white matter (WM), and cerebrospinal fluid (Potts et al. 2014); (6) the functional images were normalized to the standard Montreal Neurological Institute (MNI152) template in 1.5 mm^3 by using Diffeomorphic Anatomical Registration Through Exponentiated Lie algebra (DARTEL, (Ashburner 2007) toolbox); (7) the masks of CSF and WM were defined by thresholding individual tissue probability maps at 0.99. The first five principal components from each of the CSF and WM masks were regressed out from time series of every voxel; (8) a band-pass filter ranging from 0.01 to 0.1 Hz was applied to the time

series of each voxel. A 3-mm Gaussian kernel was used to smooth the functional images excluded the BF regions.

The Mask of Basal Forebrain

Using histological sections obtained from 10 postmortem brains (Zaborszky et al. 2008), the individual components of the magnocellular groups of the BF were delineated, 3D reconstructed, and warped to the single subject reference space of the MNI coordinates (Collins et al. 1994; Holmes et al. 1998). The definition of the various subdivisions used here (Ch1-2 = mask 1; Ch3 = mask 2; Ch4 = mask 3; Ch4p = mask4; Zaborszky et al. 2008) follows a much simpler scheme than the original subdivisions proposed by Mesulam (Mesulam et al. 1983), as in many instances it is not possible to consistently define boundaries between individual compartments, which was noted in 1988 in a symposium on nomenclature of the BF system (Butcher and Semba 1989). Each individual compartment has a stereotaxic probabilistic map, which ranges from 0 to 10 indicating the number of brains from which specific magnocellular cell groups overlap in a specific voxel. In order to remove small overlaps between each subcompartment's mask, winner-takes-all (WTA) maps (Fig. 1*B*) were obtained by labeling each voxel to the subcompartment of the highest probabilistic value. Then, all WTA maps were thresholded at 50%. We down-sampled these maps into 1.5 mm per voxel as the functional images.

Parcellation Analysis

To explore the functional segregation of BF areas, we parceled the 50% of the left and right BF volume. Functional correlation maps were calculated by correlating each voxel within the BF to the rest of the brain. All functional correlation maps were Fisher's *Z*-transformed. For each subject, eta^2 value was obtained for each pair of voxels' *z*-transformed functional correlation maps, which resulted in an eta^2 similarity matrix. Then we performed 3 sets of clustering analysis. The first set of eta^2 matrix is based on the left BF from 2 scanning sessions. The second set is based on the right BF from 2 scanning sessions. For each set, the averaged eta^2 similarity matrix was parceled into 2–15 clusters. To achieve a stable result, we performed the spectral cluster analysis 100 times on each set. The optimal cluster solution was based on 2 widely used topological criterions: variation of information (VI, (Meilă 2003)) and Hartigan metric (Hartigan 1985). The variation of information has been used to measure the similarity between the cluster *K* and cluster *K* + 1. A good solution *K* showed a significant decrease in VI from *K*–1 to *K* or significant increase from *k* to *K* + 1 (a gap pattern). Variation of information is defined as:

$$VI(C_{k-1}, C_k)_k = H(C_{k-1}) + H(C_k) - 2MI(C_{k-1}, C_k),$$

where *H* represents the entropy of the cluster solution C, and MI represents the mutual information shared by the 2 cluster solution.

Hartigan metric (Hartigan 1985) is commonly used as an index to estimate the relative change of model fitness as number of clusters changes. If *k* is the result of *k* clusters and *k* + 1 is the result of *k* + 1 clusters, then it is justifiable to add the extra cluster when Hartigan value is higher than 10. Thus, the smallest value below 10 indicates the best solution. The other option would be looking at the elbow points of the curve.

$$hartigan_k = \left(\frac{trW_k}{trW_{k+1}} - 1\right)(n - k - 1)$$

W_k is the within cluster distance at the cluster *K* based on cosine similarity. We calculated all the criteria for each cluster size and each voxel-term matrix. By applying rules as

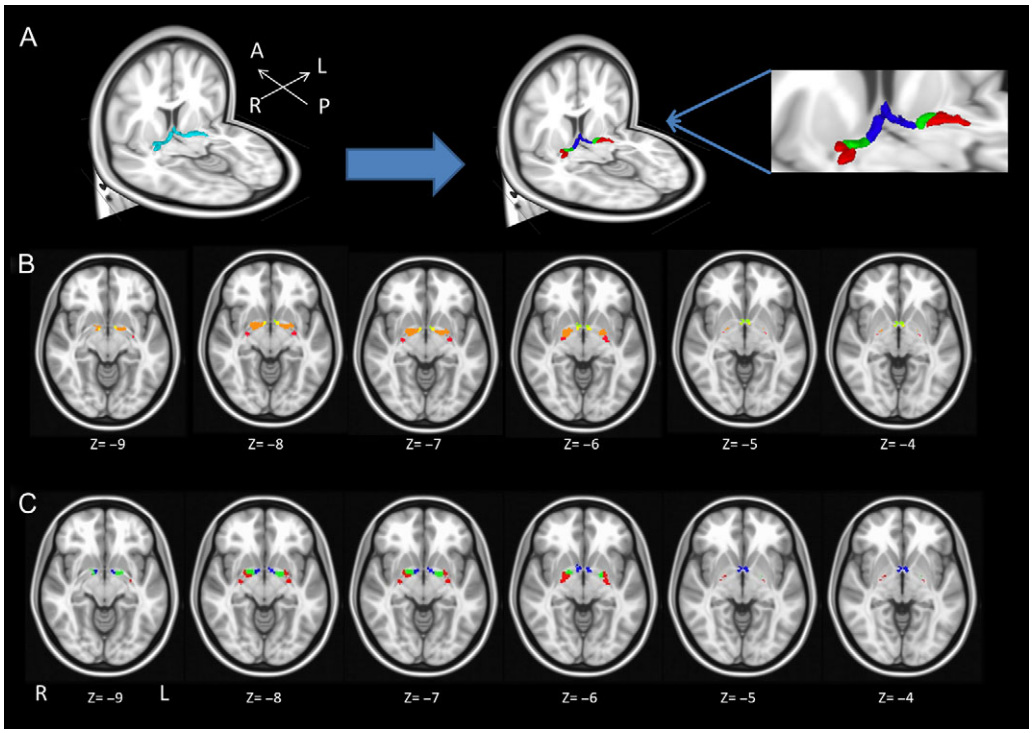

Figure 1. Illustrates the location and subdivisions of the human BF. (*A*) 3D view of functional BF subdivisions as delineated by this study. (*B*) the 50% winner-takes-all clusters on MNI template from Zaborszky et al. (2008). (*C*) the axial view of BF functional subdivisions that are derived from this study.

mentioned above, the optimal solution is decided for left and right as well as the whole BF (Supplementary Fig. S1). Finally, we performed spectral clustering with the optimal cluster size on averaged conjunction matrices of whole BF to generate the final parcellation map of the BF.

Seed-Based Correlation

Seed time series were extracted by averaging all voxels from each cluster of the parcellation map. All seeds were orthogonalized to each other by the Gram–Schmidt process. We calculated the correlation coefficient between each orthogonalized seed with the time series of all other voxels within the whole-brain GM mask, resulting in functional correlation maps for each compartment. All functional correlation maps were Fisher's z-transformed. One-sample *t*-tests were performed on z-transformed correlation maps of each subcompartment.

Test-Retest Reliability of Resting-State Connectivity on Each Subdivision

To test whether the voxels that are significant during the test are still significant during the second session, 2 approaches were used to secure the reliability of the results. Based on the one-sample *t*-test from each session, a formal conjunction analysis was conducted with hypothesizing the conjunction null. A voxel-based family-wise correction of $P < 0.05$ was used to correct the multiple comparisons. Jaccard index was calculated to find the percent of voxels that are shared across various thresholds of one-sample *t*-test results.

Meta-Analysis Co-Activation Modeling and Decoding

If these subregions identified by the clustering analysis reflect meaningful functional divisions, they should emerge not only in time course-based analysis but also in large-scale analysis of entire studies. Neurosynth is the largest open-access database which comprises reported activations from around 10 000 previous studies. We downloaded the latest version of the Neurosynth dataset (https://github.com/neurosynth/neurosynth)(v5). First, studies (including PET and fMRI) in the Neurosynth database that reported activation within each subcompartment of BF were obtained. All those coordinates in Talairach space were converted into MNI space by using (tal2ichm). Each voxel in the binary database was coded as 1 if it fell within the 10-mm focus reported in the study (Wager et al. 2009; Yarkoni et al. 2011). The co-activation map in each cluster of BF space was estimated by a multiple logistic regression (presence vs. absence). Each map was thresholded using FDR corrected $P < 0.05$. To decode the psychologic process associated with each subcompartment of the BF, we measured the dice coefficient between each co-activation map with the reverse inference co-activation maps from four sets of topics. The top five unique topics from each cluster were listed.

Results

Functional Parcellation of the Magnocellular Groups of the Basal Forebrain

Based on the functional profile of each voxel, this data-driven approach divided the magnocellular groups of the entire BF cholinergic space as delineated by Zaborszky et al. (2008) into 3 compartments (clusters) along the rostral–caudal axis of the BF (Fig. 1A), and the cluster size was optimized across subjects and 2 fMRI sessions (Supplementary Fig. S1). Here, to avoid misunderstanding, the compartments delineated in the postmortem study (Zaborszky et al. 2008) are referred to as *Ch masks*; when referring to the Ch compartments by Mesulam, only the alphanumeric signs are used (Ch1-2; Ch3; etc.). Volumes delineated in the current functional study are termed clusters or compartments. The spatial distribution of clusters can be seen in transversal planes of Figure 1C. The rostral subdivision (cluster 1, blue in Fig. 1A and C) encompassed 100% of the Ch1-2 mask and 100% of the Ch3 mask, as well as about 6% of the Ch4 mask. The middle subdivision (cluster 2, green) is composed of about 54% of the Ch4 mask, and the caudal subdivision (cluster 3, red) covered 40% of Ch4 and 100% of the Ch4p mask (Table 1). These derived clusters were concordantly organized in both hemispheres.

Functional Connectivity with Specific Cortical or Subcortical Regions

As shown in Figure 2 and Table 2, spontaneous activity of the rostral compartment (cluster 1) was positively associated with several cortical regions, including the anterior cingulate cortex [BA24/32/25], the parahippocampal region [BA28/35], the insula [BA13], the superior [BA22] and middle temporal gyrus [BA21], the middle frontal gyrus [BA11], the inferior frontal gyrus [BA47] and the posterior cingulate cortex/precuneus [BA31] (Fig. 2, Table 2). The mediodorsal nucleus (MDN), medial geniculate nucleus (MGN), and the pulvinar of the thalamus were positively correlated with this cluster. The middle compartment (cluster 2) was significantly connected to the lateral globus pallidus, putamen, caudate, and several cortical areas, including the mid-cingulate cortex [BA24/32], the insula [BA13], middle and inferior frontal gyrus [B/47], and the parahippocampal gyrus [BA27] (Fig. 2, Table 3). In the thalamus, in addition to the MDN, the anterior (AN), and ventral anterior nucleus (VAN) also displayed positive association. The caudal compartment (cluster 3) was significantly correlated with the lentiform nucleus, (putamen and globus pallidus), the entorhinal and retrosplenial cortex (BA28/30), the thalamus, the cerebellum, claustrum, insula, the precentral gyrus [BA4/6], and the middle and inferior frontal gyrus [BA6/] (Fig. 2; Table 4). The detailed slice-wise view of functional connectivity maps within each session is illustrated in Supplementary Figs S2–S4. These results demonstrated high test-retest reliability. The overlaps (dice coefficients)

Table 1. Overlaps between the data-driven parcellation based on RSFC and the individual compartment of the magnocellular groups of the BF. Panel A shows the number of overlapped voxels between data-driven cluster and the BF masks. Panel B illustrates the percentage of the number of overlapped voxels versus the size of each mask

	Mask 01 (Ch1-2)	Mask 02 (Ch3)	Mask 03 (Ch4)	Mask 04 (Ch4p)
A: overlapped voxels				
Cluster 1	63	43	12	0
Cluster 2	0	0	99	0
Cluster 3	0	0	73	52
B: overlapped percentage				
Cluster 1	1	1	0.06	0
Cluster 2	0	0	0.54	0
Cluster 3	0	0	0.40	1

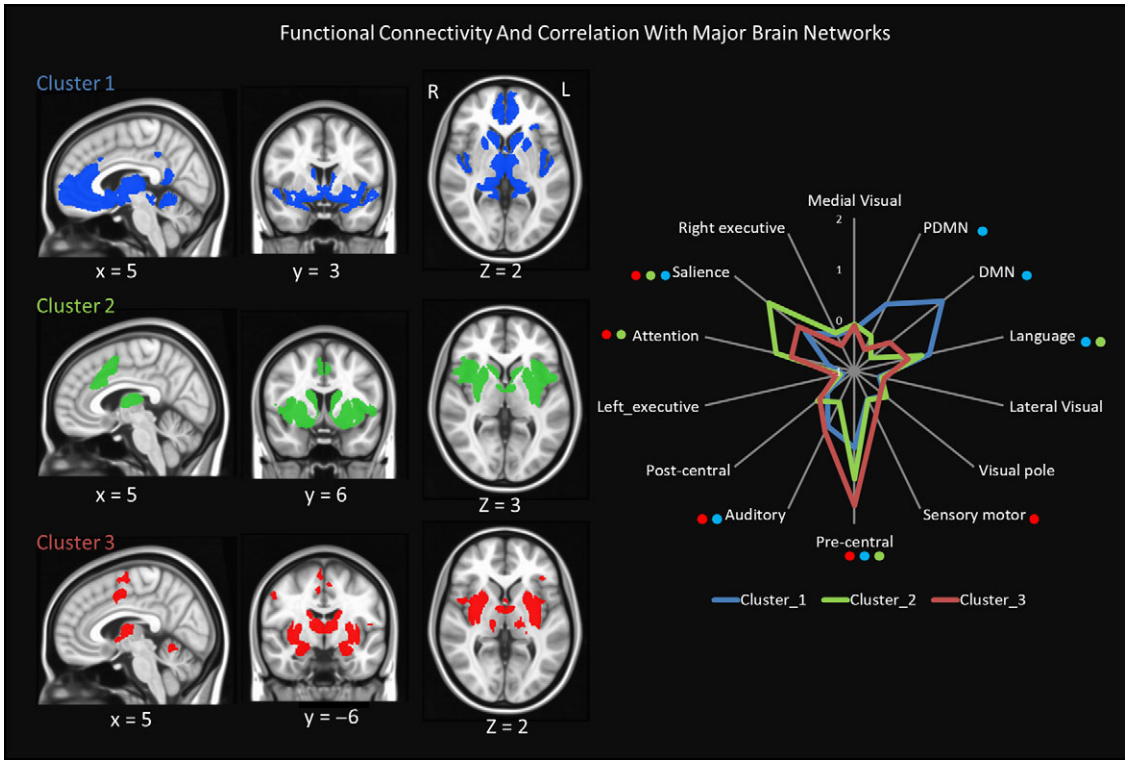

Figure 2. Functional connectivity of individual subdivision and its relation with major networks. The significantly correlated regions of each cluster were rendered on MNI standard space (FWE corrected $P < 0.05$) on the left-hand size. The functional connection between each cluster and major networks is shown on the graph at right-hand side. The averaged strength of association is based on the first fMRI session. Only the significant associations (FDR $P < 0.05$) at both sessions are indicated next to each network by color-coded dots.

Table 2. Conjunction analysis results of the group-level functional connectivity of cluster 1. Clusters are thresholded at $P < 0.05$, and the minimum cluster size is 20

Cluster size	MNI coordinates (mm)			T-value	Side	Anatomical region	BA
	X	Y	Z				
31 318	0	3	−2	53.65	L	Caudate	*
	6	36	−6	14.78	R	Anterior Cingulate	24
	−6	28	−9	13.83	L	Anterior Cingulate	24
	−3	33	−3	12.92	L	Anterior Cingulate	24
	−2	34	4	12.3	L	Anterior Cingulate	24
	−2	45	−8	12.03	L	Anterior Cingulate	32
	−3	40	3	11.84	L	Anterior Cingulate	32
	−10	40	−10	10.87	L	Anterior Cingulate	32
	−15	−30	−6	12.85	L	Thalamus (MGN)	*
	2	−9	8	11.39	L	Thalamus (MDN)	*
	22	−34	3	10.97	R	Thalamus (Pulvinar)	*
	28	−24	−15	12.07	R	Parahippocampal Gyrus	28
	20	−30	−8	11.03	R	Parahippocampal Gyrus	35
	−39	4	−12	11.38	L	Insula	13
	−48	−2	−6	11.27	L	Superior Temporal Gyrus	22
	16	−26	−8	10.9	R	Basal forebrain	*
211	60	−10	−15	7.09	R	Middle Temporal Gyrus	21
	54	−12	−12	6.84	R	Superior Temporal Gyrus	22
113	0	−40	40	6.71	L	Precuneus	31
40	−26	45	−15	7.02	L	Middle Frontal Gyrus	11
27	44	21	−12	6.6	R	Inferior Frontal Gyrus	47
	48	21	−8	6.32	R	Inferior Frontal Gyrus	47
	40	20	−15	6.17	R	Inferior Frontal Gyrus	47

*Means that there is no corresponding Brodmann area for this region.

Table 3. Conjunction analysis results of group-level functional connectivity of cluster 2. Clusters are thresholded at $P < 0.05$, and the minimum cluster size is 20

Cluster size	MNI coordinates (mm)			T-value	Side	Anatomical region	BA
	X	Y	Z				
14 561	21	3	−8	40.05	R	Lateral Globus Pallidus	*
	−20	−3	−10	33.88	L	Lateral Globus Pallidus	*
	−22	0	−9	39.53	L	Putamen	*
	−12	9	4	17.66	L	Caudate	*
	−10	9	0	17.18	L	Caudate	*
	15	14	3	15.24	R	Caudate	*
	12	3	10	14.17	R	Caudate	*
	−8	4	−2	12.15	L	Caudate	*
	−14	−4	16	11.09	L	Caudate	*
	−8	−3	6	13.41	L	Thalamus (VAN)	*
	10	−2	10	12.97	R	Thalamus (AN)	*
	2	−12	12	11.23	L	Thalamus (MDN)	*
	15	−8	15	10.07	R	Thalamus	*
	44	15	−3	11.95	R	Insula	13
	−39	14	−2	10.46	L	Insula	13
	32	8	8	10.6	R	Claustrum	*
1675	−2	9	45	8.51	L	Cingulate Gyrus	24
	3	9	45	8.24	R	Cingulate Gyrus	24
	3	18	39	7.57	R	Cingulate Gyrus	32
	10	18	30	7.55	R	Cingulate Gyrus	24
	−2	20	38	7.41	L	Cingulate Gyrus	32
	−2	24	30	7.1	L	Cingulate Gyrus	32
	−3	30	22	6.82	L	Cingulate Gyrus	32
	−8	20	28	6.62	L	Cingulate Gyrus	24
	6	14	46	8.09	R	Medial Frontal Gyrus/dorsal anterior cingulate	32
21	−24	33	−12	6.98	L	Inferior Frontal Gyrus	47

*Means that there is no corresponding Brodmann area for this region.

across different threshold *t* maps between 2 sessions were as high as 0.8 (Supplementary Fig. S5). The dice coefficients of percentile *t* map only plummeted when those maps were thresholded at extreme levels (Supplementary Fig. S5).

Functional Connectivity with Major Brain Networks

The connections between each cluster and well-defined resting-state networks were also measured. As shown in Fig. 2, these subdivisions were preferably connected with different resting-state networks. Cluster 1 was significantly associated with the default mode network (DMN), posterior default mode (PDMN), salience network, auditory and language networks, as well as premotor (precentral) network. Cluster 2 was significantly connected with the salience, attention, language, and premotor networks. Cluster 3 was preferentially correlated with the sensory-motor, premotor, attention, salience and auditory networks. However, based on the average association strength, cluster 2 was more strongly associated with salience and attention networks, while cluster 3 was more strongly associated with premotor and sensory-motor networks.

Meta-Analytic Co-Activation Networks of Each Subdivision

To further confirm the connectivity pattern of each compartment of the BFcs, we performed meta-analysis based on the Neurosynth dataset. The meta-analytic connectivity modeling (MACM) measures the co-activation patterns of a seed region across a large number of neuroimaging studies. The underlying assumption is that if 2 regions are reported together across studies, there is a very good chance that they are co-activated, and might indicate that these 2 regions are functionally connected. The meta-analytic co-activation analysis identified similar patterns as found in the RSFC analysis (compare Fig. 2 with Fig. 3), although the co-activation regions only partially overlapped with that of RSFC. The co-activation regions of cluster 1 were along the orbital gyrus [BA11], fusiform gyrus [BA 20], middle and inferior frontal gyrus [BA47], rectus gyrus [BA11], the inferior temporal gyrus, and the hypothalamus. Cluster 2 was coupled with the basal ganglia, the thalamus, the right superior frontal, and the anterior cingulate gyrus [BA24]. Cluster 3 was coupled with the supplementary motor area (SMA), precentral gyrus, the inferior temporal gyrus, the inferior frontal gyrus, and the declive of the cerebellum.

Decoding of Basal Forebrain Subdivisions

As previous studies have introduced, correlating each meta-analytic insula co-activation map with the reverse inference meta-analytic map is an effective way to decode mental states from functional networks of brain regions (Yarkoni et al. 2011). We followed the same procedure, except instead of choosing single set of topics, we measured the correlation with 200 topics (Supplementary Fig. S5), as well as 50 topics, 100 topics, and 400 topics (Supplementary Fig. S6). According to the 200 topics set, the cluster 1 was associated with learning-related topics such as “decision choice,” “feedback_error,” and “feedback_learning”; and also reward-related topics such as “reward motivation,” “drug_cocaine,” “alcohol drug,” “food_obese,” and “food_taste.” Cluster 2 was mainly correlated with emotion-

Table 4. Conjunction analysis results of group-level functional connectivity result of cluster 3. Clusters are thresholded at $P < 0.05$, and the minimum cluster size is 20

Cluster size	MNI coordinates (mm)			T-value	Side	Anatomical region	BA
	X	Y	Z				
3086	−27	−8	−6	26.37	L	Lentiform Nucleus	*
	−28	−3	−12	25.4	L	Lentiform Nucleus	*
	−28	−18	8	14.2	L	Lentiform Nucleus	*
	−32	−21	8	11.73	L	Lentiform Nucleus	*
	−32	4	6	10.25	L	Claustrum	*
	−30	−24	10	8.96	L	Claustrum	*
	−33	−12	10	7.94	L	Claustrum	*
	−30	6	10	7.9	L	Claustrum	*
	−33	−8	10	7.7	L	Claustrum	*
	−42	4	8	6.16	L	Insula	13
	−46	8	−2	6.07	L	Insula	13
3639	27	−4	−6	26.2	R	Putamen	*
	28	2	−9	23.18	R	Putamen	*
	32	6	9	10.72	R	Putamen	*
	28	−10	−6	25.33	R	Lateral Globus Pallidus	*
	27	−16	−14	10.04	R	Lateral Globus Pallidus	*
	21	−4	−9	23.92	R	Medial Globus Pallidus	*
	21	−14	−14	9.86	R	Parahippocampal Gyrus	28
	18	−32	−6	7.24	R	Parahippocampal Gyrus	30/27
	33	−10	14	9.22	R	Claustrum	*
	32	−22	10	8.61	R	Claustrum	*
	21	−27	−6	8.62	R	Medial Geniculum Body	*
	33	−20	8	8.59	R	Lentiform Nucleus	*
	42	4	8	8.35	R	Insula	13
	50	2	8	7.06	R	Insula	13
	15	−24	−3	7.97	R	Mammillary Body	*
	16	−26	−8	7.8	R	Basal forebrain	
2290	16	−6	20	11.97	R	Caudate Body	*
	2	3	−3	11.8	L	Caudate Head	*
	−16	−14	21	10.73	L	Caudate Body	*
	−18	−18	21	10.73	L	Caudate Tail	*
	20	−21	21	8.86	R	Caudate	*
	−20	−26	21	8.47	L	Caudate	*
	12	−3	12	10.67	R	Thalamus (AN)	*
	−9	−4	10	9.69	L	Thalamus (AN)	*
	−2	−6	8	9.54	L	Thalamus	*
	−18	−21	16	9.26	L	Thalamus (LPN)	*
	−16	−15	16	9.15	L	Thalamus (VLN)	*
	−16	−10	15	8.46	L	Thalamus (VLN)	*
	−21	−22	10	8.39	L	Thalamus (Pulvinar)	*
	18	−16	16	7.93	R	Thalamus (LPN)	*
	21	−21	14	7.84	R	Thalamus (VPN)	*
	−20	−20	3	7.75	L	Thalamus (VpLN)	*
312	10	2	46	8.58	R	Cingulate Gyrus	24
249	12	−52	−14	7.18	R	Culmen	*
	6	−56	−10	6.7	R	Culmen	*
	2	−63	−14	6.09	R	Declive	*
80	3	−6	63	6.59	L	Medial Frontal Gyrus	6
	6	0	63	6.44	R	Medial Frontal Gyrus	6
62	56	−3	42	6.81	R	Precentral Gyrus	4
37	−51	−3	10	6.7	L	Precentral Gyrus	6
	−46	−3	12	6.41	L	Insula	13
31	−6	−6	52	6.38	L	SMA	6
22	−39	30	3	7.05	L	Inferior Frontal Gyrus	47

*Means that there is no corresponding Brodmann area for this region.

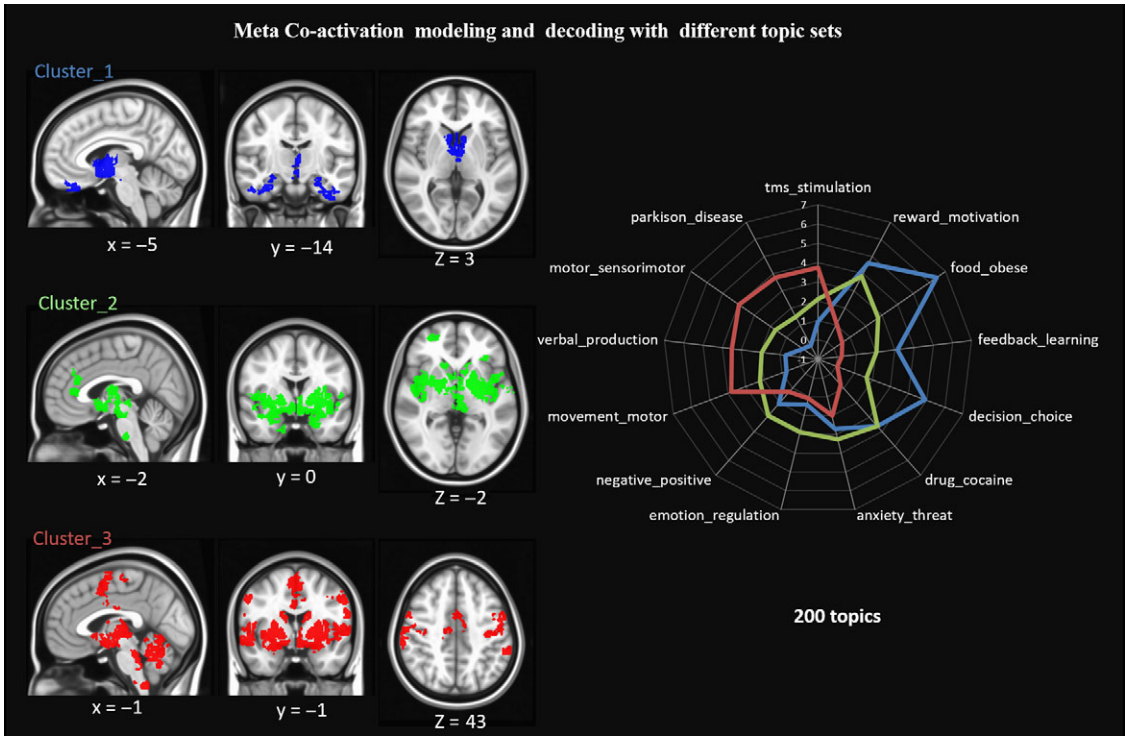

Figure 3. Co-activation map of each cluster and its functional profiles. For each cluster, thresholded whole-brain co-activation maps were generated (FDR corrected $P < 0.05$ and cluster size >200 mm^3). All maps were rendered on MNI template. Based on 200 topics, each cluster was profiled to its most preferred topics. Each cluster showed distinct functional preference. The dice coefficients were further fisher-Z scored.

related topics, such as "emotional_faces," "emotional_negative," and "anxiety_threat." Cluster 3 was associated with motor-related topics, like "motor_movement," "motor_sensorimotor," "force_motor," and "Parkinson_disease."

Significant Overlaps and Segregation of Cortical Projections from Each Subdivision

The functional connection of each compartment showed complex functional connectivity patterns where both segregation and overlaps were observed (Fig. 4). For example, the insula was related to all 3 compartments; cluster 1 was associated primarily toward the ventral part of the insula. Cluster 2 was linked to the dorsal section of the insula, and cluster 3 was related to the posterior portion. As for the cingulate gyrus, cluster 1 was highly associated with the rostral anterior cingulate cortex, while cluster 2 was correlated with the dorsal cingulate cortex. Cluster 3 was correlated with part of the cingulate motor cortex and the SMA. In general, functional connectivity between the cingulate cortex and BF clusters was organized along the anterior to posterior axis. The hippocampus has long been reported to be connected with BFcs (Mesulam et al. 1983), and here all 3 clusters were significantly connected with the hippocampus. The functional connectivity of the first cluster showed the largest spatial extent in the hippocampus, and it comprised the majority of the CA1 subdivision in the ventral part of the hippocampus. The functional connectivity of cluster 2 and cluster 3 was mainly related to the dorsal part of the hippocampus, which corresponded to the CA2 and CA3 subdivisions. Thus, the functional connectivity of all clusters overlapped in the dorsal

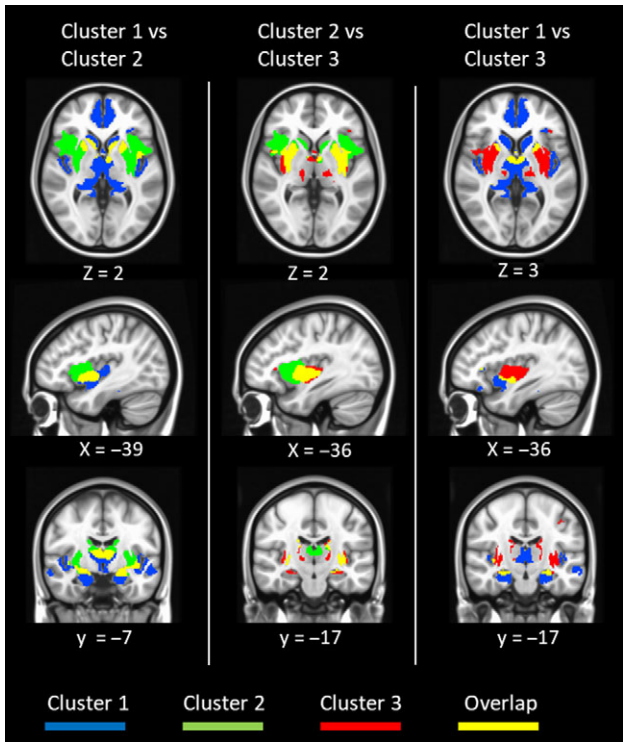

Figure 4. The overlaps and differences between functional connectivity of each cluster. The first column illustrates overlaps between cluster 1 and cluster 2. The second column demonstrates overlaps between cluster 2 and cluster 3. The third column shows overlaps between cluster 1 and cluster 3.

part of the hippocampus, but only cluster 1 was functionally connected to the ventral part of the hippocampus (Fig. 4). Additionally, all clusters were functionally connected with the thalamus (Fig. 4). Cluster 1 was shown to have functional connectivity to the largest portion of the thalamus, including the AN, MDN, and pulvinar; while cluster 2 was only significantly correlated with the AN. Cluster 3 was correlated with the posterior lateral nucleus.

Discussion

Based on high-resolution fMRI, this study demonstrates that the human BFcs comprises at least 3 compartments with distinct patterns of large-scale functional connectivity. These results illustrate a continuous projection from the BF to the medial prefrontal cortex, cingulate cortex, and precuneus. Moreover, each compartment showed a distinct connectional pattern. Meta-analysis was also utilized to infer its divergent contributions to human cognition and behavior. Cluster 1 was preferentially related to topics such as reward, decision. Cluster 2 was involved with emotion-related topics, and cluster 3 was associated with topics related to motor movement.

Functional Cluster Correspondence with the Stereotaxic Probabilistic Masks

The Ch nomenclature was proposed by Mesulam et al. (1983) to delineate the cholinergic neurons based on their topography in the BF and their cortical projection pattern. Cholinergic cells in the medial septum and diagonal band of Broca that project to the hippocampus were designated as Ch1 and Ch2, respectively. The Ch3 group was used to refer a band of fusiform neurons that are close to the ventral surface of the brain in the subcommissural area and project to the olfactory bulb (Mesulam and Geula 1988; Mufson et al. 1989). Those cholinergic cells projecting to the major part of the cortex and amygdala were termed as Ch4. The Ch4 compartment was further divided into six subdivisions; however, most of those delineations on standardized MRI were impractical and difficult to reproduce due to lack of specific landmarks (Zaborszky et al. 2008, 2015). For example, there is no clear boundary in the septum between Ch1 and Ch2. Similarly, it is difficult to delineate the various subdivisions within the Ch4 group. To avoid arbitrary delineation Zaborszky et al. (2008, 2015) and colleagues combined Ch1 and Ch2 as mask Ch1-2 together. In this latter probabilistic stereotaxic delineation map, the Ch3 mask represents a transitory area between the septum–diagonal band complex and the major part of BNM; mask Ch4 corresponds to BNM and mask Ch4p represents a well-defined posterior cell group behind the supraoptic nucleus where the optic tract attaches to the internal capsule/cerebral peduncle. These subdivisions are defined solely on topographic grounds without reference to projection targets. Interestingly, the functional parcellation scheme combines Ch1, Ch2, and Ch3 masks all together into cluster 1. Cluster 2 represents the anterior part of the Ch4 mask, and cluster 3 consists of the caudal part of the Ch4 mask and the entire Ch4p mask. In this current study, the functional parcellation follows a rostrocaudal pattern, although there are fewer functional subdivisions than the original postmortem stereotaxic delineation map.

As several studies have shown, the spectral cluster analysis is relatively robust as compared with other clustering methods, and it has been widely used in neuroimaging studies (Kelly et al. 2012; Bzdok et al. 2013; Chang et al. 2013). However, any clustering algorithm is inevitably embedded with biases that affect clustering solutions concerning the number, shape, relative size, and contiguity of the clusters. While the cluster validity problem is an unresolved issue in several scientific fields, such as pattern recognition and machine learning, and the current clustering solution might not fully reflect the underlying functional segregation of the BFcs, it still can shed a light on the functional division of this tiny structure, and provides a general understanding of its inner architecture. Future high-resolution fMRI studies may reveal more detailed functional subdivisions such as proposed in the rodent BFcs.

Functional Connectivity of BFcs Compartments with Specific Cortical or Subcortical Regions

Corticopetal cells projecting to specific cortical areas in monkeys form longitudinal bands along the rostromedial–caudolateral axis of the BF (Pearson et al. 1983), while projection cells are not homogeneously distributed but show high-density cell aggregates with some topography (Mesulam and Van Hoesen 1976; Mesulam et al. 1983; Mesulam and Geula 1988; Zaborszky et al. 2015). For example, the hippocampus primarily receives its cholinergic projection from the medial septum and the diagonal band of Broca (Ch1-2); the subgenual and dorsal anterior parts of the cingulate cortex (corresponding to BA 25, 32, 24 in humans) is innervated from the Ch4am of Mesulam, and the auditory association areas corresponding to BA 20, 21 in the superior and middle temporal gyrus in humans receive their cholinergic projection from the Ch4p compartment of Mesulam. Moreover, cells projecting to widely separated cortical areas often overlap in the monkey BF (Pearson et al. 1983; Ghashghaei and Barbas 2001). In a detailed quantitative study of the rodent BF, it was shown that the extent of overlap between 2 randomly chosen populations in the BF correlates with the strengths of cortico-cortical interconnections of the projection targets of these 2 populations (Zaborszky et al. 2015). Also, the same cortical target region may receive projections from more than one BF cell group; for example, the same part of the orbitofrontal cortex receives projections from the horizontal limb of the diagonal band as well as from various compartments of the BNM in monkeys (Ghashghaei and Barbas 2001). The interpretation of the RSFC is further complicated by the fact that functional connectivity reflects not only mono-, but also polysynaptic anterograde and retrograde connections (Skudlarski et al. 2008; Honey et al. 2010).

Although the functional connectivity of each cluster has shown a unique pattern on a large-scale, there are some interesting local separations and overlaps between each cluster's functional projections (Fig. 4). For instance, the insula in primates is strongly connected with Ch4 with a cascading pattern (Mesulam et al. 1983; Mesulam and Geula 1988), in which the anterior insula is highly connected with the intermediodorsal Ch4 compartment (Ch4id); the middle insula is connected with an anterior Ch4 compartment (Ch4ai) and the posterior insula is connected with an intermedioventral Ch4 (Ch4iv) compartment. The current study has shown that the insula is linked to all 3 clusters; cluster 1 was associated more toward the ventral part, cluster 2 linked to the middle-dorsal section, and cluster 3 was related to the posterior portion (Fig. 4). RSFC association of BF clusters generally corresponds to the functional segregation of the insula as suggested by Klein et al. (2013). As shown in Fig. 4, the functional projections from cluster cluster1 and cluster 2 were highly overlapped at the thalamic VA/AN, which have a reciprocal connection with prefrontal regions and are

highly related with DMN, and also the salience and executive networks (Yuan et al. 2016). Cluster 3 was functionally connected to the VL nucleus, and had no overlap with other clusters' projection. The VL nucleus forms a major portion of the motor thalamus. In monkeys, it receives input from the globus pallidus and cerebellum and projects to the premotor cortex (Sakai et al. 2000). The mediodorsal thalamic nucleus (MDN) was linked to both cluster 1 and cluster 2, supporting rodent data showing that the MDN receives a projection from the BF (Young et al. 1984). It is possible that BF connections may play a crucial role in the control of thalamic functions. However, since the only cholinergic and GABAergic projections from the BF that have been found are to the MDN (Young et al. 1984; Asanuma 1989) and the reticular thalamic nucleus (Asanuma 1989; Pita-Almenar et al. 2014), the functional connectivity to VA/VL might be due to indirect connection. Nevertheless, all clusters are strongly connected with certain parts of the striatum, such as the caudate head, globus pallidus, and putamen, following a rostral to caudal organization and medio-lateral arrangement. The human striatum has been shown to be involved in a large array of brain functions, such as reward-related processes, emotional regulation, and sensorimotor processes (Choi et al. 2012; Pauli et al. 2016). The BF and the striatum are adjacent structures with several functional overlaps. For instance, cluster 1 shows greater connection with caudate head compared with cluster 3. Both cluster 1 and caudate head are shown to be related to reward functions. However, the striatum itself has a complex functional and structural organization. It would be difficult to infer BF's functions solely based on functional connectivity with subcortical structures.

Functional Relation of BF Subcompartments with Major Brain Networks

Functional studies on human brains have identified several major functional networks, which also correspond to regions co-activated by various tasks (Biswal et al. 1995; Dosenbach et al. 2007; Smith et al. 2009; Power et al. 2010; Yeo et al. 2011; Choi et al. 2012). In the current study, we explored the relationship between each BF subdivision and major resting networks (Fig. 2).

Cluster 1

Was highly correlated with the DMN and PDMN. The DMN might be the most extensively studied network in humans, which shows enhanced activation during rest and reduced activation during attention-demanding tasks (Shulman et al. 1997; Raichle et al. 2001; Buckner et al. 2008). DMN also seems to be associated with a wide range of cognitive functions, such as memory, consciousness, and self-reflection (Gusnard et al. 2001; Buckner et al. 2008; Christoff et al. 2009). Procholinergic drugs suppressed activity in regions that highly overlap with the DMN (Ghatan et al. 1998; Bentley et al. 2011). Therefore, the association between cluster 1 and DMN might occur simply due to the anatomical connection between cholinergic neurons in cluster 1 and the hippocampus, cingulate cortex, and precuneus. Many of the same studies have shown that cholinergic stimulation increases task-related activity in dorsolateral frontal and posterior parietal regions, suggesting that the BF shifts processing from the default network to attentional-sensory systems. However, imaging studies using systemic cholinergic pharmacological challenges must be interpreted cautiously, because the drugs used will affect every brain region containing the respective receptors and changes in brain activity may occur downstream from the initial site of pharmacological action. In fact, it has been shown that glutamatergic axon terminals originating in the anterior cingulate cortex (ACC/BA 32) contain m2-muscarinic receptors and synapse on inhibitory and pyramidal neurons in the dorsolateral prefrontal cortex (DLPFC/BA 9). Thus, cholinergic mechanisms play a complex role in the opposite activation pattern between ACC and DLPFC; the action of specific presynaptic receptors must be considered in addition to the state-dependent modulations in ACC/DLPFC by the quantitatively differing ascending BF projections to ACC and DLPFC (Medalla and Barbas 2012). Interestingly, both reduced activation of DMN (Sorg et al. 2007; Buckner et al. 2008; Palop and Mucke 2010) and loss of neurons in BNM (Iraizoz et al. 1991; Lehericy et al. 1993) were reported to occur in Alzheimer's disease, and volume changes in different BF compartments have been shown to correlate with cognitive decline in MCI patients (Grothe et al. 2010). Although the Ch1-2 compartment, which projects to hippocampus, seems to have a stable amount of cells (Bigl et al. 1987), its volume shows reduction in MCI patients and this reduction is positively correlated with hippocampal atrophy (Cantero et al. 2017).

Noticeably, structures which are adjacent to cluster 1, such as the nucleus accumbens and bed nucleus of the stria terminalis (BNST), have also been reported to be functionally connected to the DMN (Cauda et al. 2011; Torrisi et al. 2015). It is possible that shared interactions with the DMN may arise due to their similar input/output relation. Otherwise, it could be because these structures are too close to current functional image resolution and most of them did define masks using microstructural details. (Zaborszky et al. 2015). Moreover, reverse inference analysis and earlier lesion studies indicate that cluster 1 is involved with reward processing and decision-making (Olmstead et al. 1998; Robledo et al. 1998).

Cluster 2

Previous animal studies support the role of the BF in processing salient and novel stimuli for reward, learning as well as cognitive motor control (Sarter et al. 2006; Paolone et al. 2013; Raver and Lin 2015). Indeed, cluster 2 was significantly correlated with the salience and attention networks (Fig. 2) and meta-analysis indicated that the cluster 2 was related with functions such as regulating and organizing neural responses to homeostatically significant stimuli (Dosenbach et al. 2007; Seeley et al. 2007), emotion (Peyron et al. 2000), and social interaction (Eisenberger et al. 2003) From a functional perspective, cluster 2 was also highly correlated with the attention network. Previous lesion studies in rats and monkeys have postulated that damage to the nucleus basalis of Meynert (cluster 2) causes impairment in attention other than memory or learning (Voytko 1996). The dorsal anterior cingulate cortex, which was functionally linked to cluster 2 in our study, participates in a sympathetic drive, while the subgenual (BA 25) cingulate cortex, which is linked cluster 1, generates antisympathetic (parasympathetic) tone (Critchley and Harrison 2013). Our study, thus, points to unexplored modulatory effects of the cholinergic system on these different autonomic mechanisms that are orchestrated from segregated BFcs clusters.

Cluster 3

Considering that cluster 3 was highly connected with motor-related networks, it is reasonable to assume that the cluster 3 is involved preferentially with motor-related functions. The reverse inference from the meta-analysis also indicated that

cluster 3 was related to motor-related clinical diseases, such as PD. Although PD is potentially caused by the degeneration of the dopaminergic cells in the substantia nigra and ventral tegmental area, cholinergic cell loss in the BF is comparable or more severe in PD and PD with dementia (PDD) than in AD cases (Muller and Bohnen 2013; Liu et al. 2015).

Interestingly, based on the functional connectivity, both cluster 1 and cluster 3 were correlated with the auditory association cortex (BA21,22). However, according to the meta-analysis, only cluster 3 co-activated with auditory associated cortex. Anatomical studies in primates and rodents also indicate that the auditory association regions receive their major projection from a caudal cholinergic cell group, located around and underneath the globus pallidus (Wenk et al. 1980; Mesulam and Geula 1988; Chavez and Zaborszky 2017). It is unclear what the cause of this discrepancy is. Considering that co-activation maps were mostly derived from task fMRI and the functional connectivity in this paper was based on resting-state fMRI, the observed mismatch might due to functional reconfiguration of the corticopetal system between task and rest.

Noticeably, the salience network, which includes 2 prominent nodes in the anterior insula and the dorsal anterior cingulate cortex that are commonly co-activated both in resting-state fMRI and a wide range of cognitive and affective tasks (Seeley et al. 2007; Menon 2015), is associated with all 3 clusters. The anterior insula (Fig. 4) and the dorsal anterior cingulate cortex (Fig. 2) were prominently linked in RSFC to cluster 2, while clusters 1 and 3 also showed significant association (FDR $p < 0.05$). The unique association of the salience network with all 3 clusters may relate to the notion that the salience network plays a dynamic switching role between the default mode and the central executive networks (Menon 2015).

Limitations and Concerns

There are several limitations in this study. First of all, this parcellation is solely based on the resting-state data and may not fully reflect its functional connectivity during tasks or even its dynamic organization. The BFcs has a complex anatomy, in which cholinergic, GABAergic and glutamatergic corticopetal neurons are intermingled to some extent with neurons of the striatopallidal and extended amygdala systems. Considering the lack of precise knowledge of the interrelationships of the various corticopetal axons in the target regions, it is expected that future imaging studies might provide a more precise parcellation and associated cortical projection patterns. In fact, recent studies in rodents using virus-based tracing (Watabe-Uchida et al. 2012; Ogawa et al. 2014; Pollak Dorocic et al. 2014; Weissbourd et al. 2014; Beier et al. 2015) suggest that each of the monoaminergic systems are organized much more specifically than previously assumed in order to modulate selective cortical areas or functions. For example, using monosynaptic virus tracing techniques in rats, it has been shown that each cortical area receives a specific set of inputs via the cholinergic corticopetal system (Gielow and Zaborszky 2017).

It is also worth mentioning that ultra-high-field 7T image provides higher resolution and higher signal-to-noise ratio, but with the drawback of more distortion and potentially more non-Gaussian noise (Yang et al. 2012). Since few studies have addressed these questions and the lack of a feasible solution, the current study followed the typical 3T image preprocessing steps similar to recent studies using 7T dataset (Bianciardi et al. 2009; Metzger et al. 2010; Lenglet et al. 2012; Torrisi et al. 2015).

Concluding Remarks

Although the BF has long been acknowledged to be anatomically heterogeneous (Burgunder and Young 1989; Heimer et al. 1991; Zaborszky et al. 1991; Benzing et al. 1993; Geula et al. 1993), most of the functional studies regarded BF as a homogeneous structure without comparing activation location with microstructural details and ignored potential functional segregation in the BFcs system. As suggested in a review almost 30 years ago (Heimer et al. 1991), the interdigitating nature of 3 macro systems of the BF, namely, the ventral striopallidal system, the extended amygdala and the magnocellular corticopetal system, may be the reason that many neuropsychiatric diseases with a site of action in this brain area result in overlapping motor disturbances, derailment of affect, motivation, and other cognitive symptoms. Recently, it has been speculated that the susceptibility of neurons in various sectors of the BF and the progression of degeneration may be specific for various degenerative diseases, including Alzheimer's and Parkinson's (Liu et al. 2015). Our study using high-resolution imaging provides a first glimpse of how distinct subdivisions of the human BFcs relate to various functional cortical networks. Given the rostrocaudal functional differences in RSFC disclosed in this study, a more rigorous assessment of the pathology in the BF with similar subdivisional functional imaging studies might help to predict the progression of AD, PD and related neurodegenerative diseases.

Supplementary Material

Supplementary material is available at *Cerebral Cortex* online.

Funding

This research was supported by NIH 5R01NS049176 (B.B.B.) and R01NS023945 (L.Z.).

Notes

Conflict of Interest: None declared.

References

Arendt T, Brückner MK, Bigl V, Marcova L. 1995. Dendritic reorganisation in the basal forebrain under degenerative conditions and its defects in Alzheimer's disease. II. Ageing, Korsakoff's disease, Parkinson's disease, and Alzheimer's disease. J Comp Neurol. 351:189–222.

Asanuma C. 1989. Axonal arborizations of a magnocellular basal nucleus input and their relation to the neurons in the thalamic reticular nucleus of rats. Proc Natl Acad Sci U S A. 86:4746–4750.

Ashburner J. 2007. A fast diffeomorphic image registration algorithm. Neuroimage. 38:95–113.

Baxter MG, Chiba AA. 1999. Cognitive functions of the basal forebrain. Curr Opin Neurobiol. 9:178–183.

Beier KT, Steinberg EE, DeLoach KE, Xie S, Miyamichi K, Schwarz L, Gao XJ, Kremer EJ, Malenka RC, Luo L. 2015. Circuit architecture of VTA dopamine neurons revealed by systematic input-output mapping. Cell. 162:622–634.

Beissner F, Schumann A, Brunn F, Eisenträger D, Bär K-J. 2014. Advances in functional magnetic resonance imaging of the human brainstem. Neuroimage. 86:91–98.

Bentley P, Driver J, Dolan RJ. 2011. Cholinergic modulation of cognition: insights from human pharmacological functional neuroimaging. Prog Neurobiol. 94:360–388.

Benzing WC, Kordower JH, Mufson EJ. 1993. Galanin immunoreactivity within the primate basal forebrain: evolutionary change between monkeys and apes. J Comp Neurol. 336: 31–39.

Bianciardi M, Fukunaga M, van Gelderen P, Horovitz SG, de Zwart JA, Shmueli K, Duyn JH. 2009. Sources of functional magnetic resonance imaging signal fluctuations in the human brain at rest: a 7 T study. Magn Reson Imaging. 27: 1019–1029.

Bigl V, Arendt T, Fischer S, Werner M, Arendt A. 1987. The cholinergic system in aging. Gerontology. 33:172–180.

Bigl V, Woolf NJ, Butcher LL. 1982. Cholinergic projections from the basal forebrain to frontal, parietal, temporal, occipital, and cingulate cortices: a combined fluorescent tracer and acetylcholinesterase analysis. Brain Res Bull. 8:727–749.

Biswal BB, Mennes M, Zuo XN, Gohel S, Kelly C, Smith SM, Beckmann CF, Adelstein JS, Buckner RL, Colcombe S, et al. 2010. Toward discovery science of human brain function. Proc Natl Acad Sci U S A. 107:4734–4739.

Biswal B, Yetkin FZ, Haughton VM, Hyde JS. 1995. Functional connectivity in the motor cortex of resting human brain using echo-planar MRI. Magn Reson Med. 34:537–541.

Bloem B, Poorthuis RB, Mansvelder HD. 2014. Cholinergic modulation of the medial prefrontal cortex: the role of nicotinic receptors in attention and regulation of neuronal activity. Front Neural Circuits. 8:17.

Buckner RL, Andrews-Hanna JR, Schacter DL. 2008. The brain's default network: anatomy, function, and relevance to disease. Ann N Y Acad Sci. 1124:1–38.

Buckner RL, Krienen FM, Castellanos A, Diaz JC, Yeo BT. 2011. The organization of the human cerebellum estimated by intrinsic functional connectivity. J Neurophysiol. 106: 2322–2345.

Burgunder JM, Young WS 3rd. 1989. Neurons with neurokinin B mRNA in the rat magnocellular basal nucleus: distribution, projection and colocalization studies. J Chem Neuroanat. 2: 239–251.

Butcher LL, Semba K. 1989. Reassessing the cholinergic basal forebrain: nomenclature schemata and concepts. Trends Neurosci. 12:483–485.

Butler T, Harvey P, Deshpande A, Tanzi E, Li Y, Tsui W, Silver C, Fischer E, Wang X, Chen J, et al. 2018. Basal forebrain septal nuclei are enlarged in healthy subjects prior to the development of Alzheimer's disease. Neurobiol Aging. 65:201–205.

Butler T, Zaborszky L, Pirraglia E, Li J, Wang XH, Li Y, Tsui W, Talos D, Devinsky O, Kuchna I, et al. 2014. Comparison of human septal nuclei MRI measurements using automated segmentation and a new manual protocol based on histology. Neuroimage. 97:245–251.

Butler T, Zaborszky L, Wang X, McDonald CR, Blackmon K, Quinn BT, DuBois J, Carlson C, Barr WB, French J, et al. 2013. Septal nuclei enlargement in human temporal lobe epilepsy without mesial temporal sclerosis. Neurology. 80:487–491.

Bzdok D, Langner R, Schilbach L, Jakobs O, Roski C, Caspers S, Laird AR, Fox PT, Zilles K, Eickhoff SB. 2013. Characterization of the temporo-parietal junction by combining data-driven parcellation, complementary connectivity analyses, and functional decoding. Neuroimage. 81:381–392.

Li C-sR, Ide JS, Zhang S, Hu S, Chao HH, Zaborszky L. 2014. Resting state functional connectivity of the basal nucleus of Meynert in humans: in comparison to the ventral striatum and the effects of age. Neuroimage. 97:321–332.

Candy J, Perry R, Perry E, Irving D, Blessed G, Fairbairn A, Tomlinson B. 1983. Pathological changes in the nucleus of Meynert in Alzheimer's and Parkinson's diseases. J Neurol Sci. 59:277–289.

Cantero JL, Zaborszky L, Atienza M. 2017. Volume loss of the nucleus basalis of Meynert is associated with atrophy of innervated regions in mild cognitive impairment. Cereb Cortex. 27:3881–3889.

Cauda F, Cavanna AE, D'Agata F, Sacco K, Duca S, Geminiani GC. 2011. Functional connectivity and coactivation of the nucleus accumbens: a combined functional connectivity and structure-based meta-analysis. J Cogn Neurosci. 23: 2864–2877.

Chang LJ, Yarkoni T, Khaw MW, Sanfey AG. 2013. Decoding the role of the insula in human cognition: functional parcellation and large-scale reverse inference. Cereb Cortex. 23:739–749.

Chavez C, Zaborszky L. 2017. Basal forebrain cholinergic-auditory cortical network: primary versus nonprimary auditory cortical areas. Cereb Cortex. 27:2335–2347.

Chiba AA, Bucci DJ, Holland PC, Gallagher M. 1995. Basal forebrain cholinergic lesions disrupt increments but not decrements in conditioned stimulus processing. J Neurosci. 15: 7315–7322.

Choi EY, Yeo BT, Buckner RL. 2012. The organization of the human striatum estimated by intrinsic functional connectivity. J Neurophysiol. 108:2242–2263.

Christoff K, Gordon AM, Smallwood J, Smith R, Schooler JW. 2009. Experience sampling during fMRI reveals default network and executive system contributions to mind wandering. Proc Natl Acad Sci U S A. 106:8719–8724.

Collins DL, Neelin P, Peters TM, Evans AC. 1994. Automatic 3D intersubject registration of MR volumetric data in standardized Talairach space. J Comput Assist Tomogr. 18:192–205.

Conner JM, Chiba AA, Tuszynski MH. 2005. The basal forebrain cholinergic system is essential for cortical plasticity and functional recovery following brain injury. Neuron. 46:173–179.

Critchley HD, Harrison NA. 2013. Visceral influences on brain and behavior. Neuron. 77:624–638.

Detari L. 2000. Tonic and phasic influence of basal forebrain unit activity on the cortical EEG. Behav Brain Res. 115: 159–170.

Dosenbach NU, Fair DA, Miezin FM, Cohen AL, Wenger KK, Dosenbach RA, Fox MD, Snyder AZ, Vincent JL, Raichle ME, et al. 2007. Distinct brain networks for adaptive and stable task control in humans. Proc Natl Acad Sci U S A. 104: 11073–11078.

Draganski B, Kherif F, Kloppel S, Cook PA, Alexander DC, Parker GJ, Deichmann R, Ashburner J, Frackowiak RS. 2008. Evidence for segregated and integrative connectivity patterns in the human Basal Ganglia. J Neurosci. 28:7143–7152.

Eisenberger NI, Lieberman MD, Williams KD. 2003. Does rejection hurt? An fMRI study of social exclusion. Science. 302: 290–292.

Everitt BJ, Robbins TW. 1997. Central cholinergic systems and cognition. Annu Rev Psychol. 48:649–684.

Fox MD, Raichle ME. 2007. Spontaneous fluctuations in brain activity observed with functional magnetic resonance imaging. Nature Rev Neurosci. 8:700–711.

Geula C, Schatz CR, Mesulam MM. 1993. Differential localization of NADPH-diaphorase and calbindin-D28k within the

cholinergic neurons of the basal forebrain, striatum and brainstem in the rat, monkey, baboon and human. Neuroscience. 54:461–476.

Ghashghaei HT, Barbas H. 2001. Neural interaction between the basal forebrain and functionally distinct prefrontal cortices in the rhesus monkey. Neuroscience. 103:593–614.

Ghatan PH, Ingvar M, Eriksson L, Stone-Elander S, Serrander M, Ekberg K, Wahren J. 1998. Cerebral effects of nicotine during cognition in smokers and non-smokers. Psychopharmacology (Berl). 136:179–189.

Gielow MR, Zaborszky L. 2017. The input-output relationship of the cholinergic basal forebrain. Cell Rep. 18:1817–1830.

Gorgolewski KJ, Mendes N, Wilfling D, Wladimirow E, Gauthier CJ, Bonnen T, Ruby FJ, Trampel R, Bazin PL, Cozatl R, et al. 2015. A high resolution 7-Tesla resting-state fMRI test-retest dataset with cognitive and physiological measures. Sci Data. 2:140054.

Granholm A-CE, Sanders LA, Crnic LS. 2000. Loss of cholinergic phenotype in basal forebrain coincides with cognitive decline in a mouse model of Down's syndrome. Exp Neurol. 161:647–663.

Grothe M, Zaborszky L, Atienza M, Gil-Neciga E, Rodriguez-Romero R, Teipel SJ, Amunts K, Suarez-Gonzalez A, Cantero JL. 2010. Reduction of basal forebrain cholinergic system parallels cognitive impairment in patients at high risk of developing Alzheimer's disease. Cereb Cortex. 20:1685–1695.

Gusnard DA, Akbudak E, Shulman GL, Raichle ME. 2001. Medial prefrontal cortex and self-referential mental activity: relation to a default mode of brain function. Proc Natl Acad Sci U S A. 98:4259–4264.

Hartigan JA. 1985. Statistical theory in clustering. J Classif. 2: 63–76.

Hedreen JC, Struble RG, Whitehouse PJ, Price DL. 1984. Topography of the magnocellular basal forebrain system in human brain. J Neuropathol Exp Neurol. 43:1–21.

Heimer L. 2000. Basal forebrain in the context of schizophrenia. Brain Res Rev. 31:205–235.

Heimer L, de Olmos J, Alheid GF, Zaborszky L. 1991. "Perestroika" in the basal forebrain: opening the border between neurology and psychiatry. Prog Brain Res. 87:109–165.

Holmes CJ, Hoge R, Collins L, Woods R, Toga AW, Evans AC. 1998. Enhancement of MR images using registration for signal averaging. J Comput Assist Tomogr. 22:324–333.

Honey CJ, Thivierge JP, Sporns O. 2010. Can structure predict function in the human brain? Neuroimage. 52:766–776.

Hur EE, Edwards RH, Rommer E, Zaborszky L. 2009. Vesicular glutamate transporter 1 and vesicular glutamate transporter 2 synapses on cholinergic neurons in the sublenticular gray of the rat basal forebrain: a double-label electron microscopic study. Neuroscience. 164:1721–1731.

Iraizoz I, de Lacalle S, Gonzalo LM. 1991. Cell loss and nuclear hypertrophy in topographical subdivisions of the nucleus basalis of Meynert in Alzheimer's disease. Neuroscience. 41: 33–40.

Jones EG, Burton H, Saper CB, Swanson LW. 1976. Midbrain, diencephalic and cortical relationships of the basal nucleus of Meynert and associated structures in primates. J Comp Neurol. 167:385–419.

Kelly C, Toro R, Di Martino A, Cox CL, Bellec P, Castellanos FX, Milham MP. 2012. A convergent functional architecture of the insula emerges across imaging modalities. Neuroimage. 61:1129–1142.

Kilgard MP, Merzenich MM. 1998. Cortical map reorganization enabled by nucleus basalis activity. Science. 279:1714–1718.

Klein TA, Ullsperger M, Danielmeier C. 2013. Error awareness and the insula: links to neurological and psychiatric diseases. Front Hum Neurosci. 7:14.

Kline RL, Zhang S, Farr OM, Hu S, Zaborszky L, Samanez-Larkin GR, Li CS. 2016. The effects of methylphenidate on resting-state functional connectivity of the basal nucleus of Meynert, locus coeruleus, and ventral tegmental area in healthy adults. Front Hum Neurosci. 10:149.

Lammers F, Mobascher A, Musso F, Shah NJ, Warbrick T, Zaborszky L, Winterer G. 2016. Effects of ncl. basalis Meynert volume on the trail-making-test are restricted to the left hemisphere. Brain Behav. 6:e00421.

Lee MG, Hassani OK, Alonso A, Jones BE. 2005. Cholinergic basal forebrain neurons burst with theta during waking and paradoxical sleep. J Neurosci. 25:4365–4369.

Lehericy S, Hirsch EC, Cervera-Pierot P, Hersh LB, Bakchine S, Piette F, Duyckaerts C, Hauw JJ, Javoy-Agid F, Agid Y. 1993. Heterogeneity and selectivity of the degeneration of cholinergic neurons in the basal forebrain of patients with Alzheimer's disease. J Comp Neurol. 330:15–31.

Lenglet C, Abosch A, Yacoub E, De Martino F, Sapiro G, Harel N. 2012. Comprehensive in vivo mapping of the human basal ganglia and thalamic connectome in individuals using 7T MRI. PLoS One. 7:e29153.

Liu AK, Chang RC, Pearce RK, Gentleman SM. 2015. Nucleus basalis of Meynert revisited: anatomy, history and differential involvement in Alzheimer's and Parkinson's disease. Acta Neuropathol. 129:527–540.

McGaughy J, Dalley JW, Morrison CH, Everitt BJ, Robbins TW. 2002. Selective behavioral and neurochemical effects of cholinergic lesions produced by intrabasalis infusions of 192 IgG-saporin on attentional performance in a five-choice serial reaction time task. J Neurosci. 22:1905–1913.

Medalla M, Barbas H. 2012. The anterior cingulate cortex may enhance inhibition of lateral prefrontal cortex via m2 cholinergic receptors at dual synaptic sites. J Neurosci. 32: 15611–15625.

Meilă M 2003. Comparing clusterings by the variation of information. In. Learning Theory and Kernel Machines Springer p 173–187.

Menon V. 2015. Salience Network. In: Toga AW, editor. Brain mapping: an encyclopedic reference, vol 2. Academic Press, Elsevier, p. 597–611.

Mesulam MM, Geula C. 1988. Nucleus basalis (Ch4) and cortical cholinergic innervation in the human brain: observations based on the distribution of acetylcholinesterase and choline acetyltransferase. J Comp Neurol. 275:216–240.

Mesulam MM, Mufson EJ, Levey AI, Wainer BH. 1983. Cholinergic innervation of cortex by the basal forebrain: cytochemistry and cortical connections of the septal area, diagonal band nuclei, nucleus basalis (substantia innominata), and hypothalamus in the rhesus monkey. J Comp Neurol. 214:170–197.

Mesulam MM, Van Hoesen GW. 1976. Acetylcholinesterase-rich projections from the basal forebrain of the rhesus monkey to neocortex. Brain Res. 109:152–157.

Metzger CD, Eckert U, Steiner J, Sartorius A, Buchmann JE, Stadler J, Tempelmann C, Speck O, Bogerts B, Abler B, et al. 2010. High field FMRI reveals thalamocortical integration of segregated cognitive and emotional processing in mediodorsal and intralaminar thalamic nuclei. Front Neuroanat. 4:138.

Mufson EJ, Bothwell M, Hersh LB, Kordower JH. 1989. Nerve growth factor receptor immunoreactive profiles in the normal, aged human basal forebrain: colocalization with cholinergic neurons. J Comp Neurol. 285:196–217.

Muller ML, Bohnen NI. 2013. Cholinergic dysfunction in Parkinson's disease. Curr Neurol Neurosci Rep. 13:377.

Ogawa SK, Cohen JY, Hwang D, Uchida N, Watabe-Uchida M. 2014. Organization of monosynaptic inputs to the serotonin and dopamine neuromodulatory systems. Cell Rep. 8:1105–1118.

Olmstead MC, Robbins TW, Everitt BJ. 1998. Basal forebrain cholinergic lesions enhance conditioned approach responses to stimuli predictive of food. Behav Neurosci. 112:611–629.

Palop JJ, Mucke L. 2010. Amyloid-beta-induced neuronal dysfunction in Alzheimer's disease: from synapses toward neural networks. Nat Neurosci. 13:812–818.

Paolone G, Angelakos CC, Meyer PJ, Robinson TE, Sarter M. 2013. Cholinergic control over attention in rats prone to attribute incentive salience to reward cues. J Neurosci. 33: 8321–8335.

Pauli WM, O'Reilly RC, Yarkoni T, Wager TD. 2016. Regional specialization within the human striatum for diverse psychological functions. Proc Natl Acad Sci U S A. 113:1907–1912.

Pearson RC, Gatter KC, Brodal P, Powell TP. 1983. The projection of the basal nucleus of Meynert upon the neocortex in the monkey. Brain Res. 259:132–136.

Peyron R, Laurent B, Garcia-Larrea L. 2000. Functional imaging of brain responses to pain. A review and meta-analysis. Neurophysiol Clin. 30:263–288.

Pita-Almenar JD, Yu D, Lu HC, Beierlein M. 2014. Mechanisms underlying desynchronization of cholinergic-evoked thalamic network activity. J Neurosci. 34:14463–14474.

Pollak Dorocic I, Furth D, Xuan Y, Johansson Y, Pozzi L, Silberberg G, Carlen M, Meletis K. 2014. A whole-brain atlas of inputs to serotonergic neurons of the dorsal and median raphe nuclei. Neuron. 83:663–678.

Potts MB, Jahangiri A, Jen M, Sneed PK, McDermott MW, Gupta N, Hetts SW, Young WL, Lawton MT, Project UBAS. 2014. Deep arteriovenous malformations in the basal ganglia, thalamus, and insula: multimodality management, patient selection, and results. World Neurosurg. 82:386–394.

Power JD, Fair DA, Schlaggar BL, Petersen SE. 2010. The development of human functional brain networks. Neuron. 67: 735–748.

Price DL, Whitehouse PJ, Struble RG. 1986. Cellular pathology in Alzheimer's and Parkinson's diseases. Trends Neurosci. 9: 29–33.

Raichle ME, MacLeod AM, Snyder AZ, Powers WJ, Gusnard DA, Shulman GL. 2001. A default mode of brain function. Proc Natl Acad Sci U S A. 98:676–682.

Raver SM, Lin SC. 2015. Basal forebrain motivational salience signal enhances cortical processing and decision speed. Front Behav Neurosci. 9:277.

Richardson RT, DeLong MR. 1991. Electrophysiological studies of the functions of the nucleus basalis in primates. Adv Exp Med Biol. 295:233–252.

Robledo P, Weissenborn R, Robbins TW, Everitt BJ. 1998. Effects of lesions of the nucleus basalis magnocellularis on the acquisition of cocaine self-administration in rats. Eur J Neurosci. 10:1946–1955.

Roy AK, Shehzad Z, Margulies DS, Kelly AM, Uddin LQ, Gotimer K, Biswal BB, Castellanos FX, Milham MP. 2009. Functional connectivity of the human amygdala using resting state fMRI. Neuroimage. 45:614–626.

Sakai ST, Stepniewska I, Qi HX, Kaas JH. 2000. Pallidal and cerebellar afferents to pre-supplementary motor area thalamocortical neurons in the owl monkey: a multiple labeling study. J Comp Neurol. 417:164–180.

Saper CB, Chelimsky TC. 1984. A cytoarchitectonic and histochemical study of nucleus basalis and associated cell groups in the normal human brain. Neuroscience. 13:1023–1037.

Sarter M, Gehring WJ, Kozak R. 2006. More attention must be paid: the neurobiology of attentional effort. Brain Res Rev. 51:145–160.

Seeley WW, Menon V, Schatzberg AF, Keller J, Glover GH, Kenna H, Reiss AL, Greicius MD. 2007. Dissociable intrinsic connectivity networks for salience processing and executive control. J Neurosci. 27:2349–2356.

Shulman GL, Fiez JA, Corbetta M, Buckner RL, Miezin FM, Raichle ME, Petersen SE. 1997. Common blood flow changes across visual tasks: II. decreases in cerebral cortex. J Cogn Neurosci. 9:648–663.

Skudlarski P, Jagannathan K, Calhoun VD, Hampson M, Skudlarska BA, Pearlson G. 2008. Measuring brain connectivity: diffusion tensor imaging validates resting state temporal correlations. Neuroimage. 43:554–561.

Smiley JF, Subramanian M, Mesulam MM. 1999. Monoaminergic–cholinergic interactions in the primate basal forebrain. Neuroscience. 93:817–829.

Smith SM, Fox PT, Miller KL, Glahn DC, Fox PM, Mackay CE, Filippini N, Watkins KE, Toro R, Laird AR, et al. 2009. Correspondence of the brain's functional architecture during activation and rest. Proc Natl Acad Sci U S A. 106: 13040–13045.

Sorg C, Riedl V, Muhlau M, Calhoun VD, Eichele T, Laer L, Drzezga A, Forstl H, Kurz A, Zimmer C, et al. 2007. Selective changes of resting-state networks in individuals at risk for Alzheimer's disease. Proc Natl Acad Sci U S A. 104: 18760–18765.

Sweeney J, Höhmann C, Oster-Granite M, Coyle J. 1989. Neurogenesis of the basal forebrain in euploid and trisomy 16 mice: an animal model for developmental disorders in Down syndrome. Neuroscience. 31:413–425.

Torrisi S, O'Connell K, Davis A, Reynolds R, Balderston N, Fudge JL, Grillon C, Ernst M. 2015. Resting state connectivity of the bed nucleus of the stria terminalis at ultra-high field. Hum Brain Mapp. 36:4076–4088.

Voytko ML. 1996. Cognitive functions of the basal forebrain cholinergic system in monkeys: memory or attention? Behav Brain Res. 75:13–25.

Voytko ML, Olton DS, Richardson RT, Gorman LK, Tobin JR, Price DL. 1994. Basal forebrain lesions in monkeys disrupt attention but not learning and memory. J Neurosci. 14:167–186.

Wager TD, Lindquist MA, Nichols TE, Kober H, Van Snellenberg JX. 2009. Evaluating the consistency and specificity of neuroimaging data using meta-analysis. Neuroimage. 45:S210–S221.

Watabe-Uchida M, Zhu L, Ogawa SK, Vamanrao A, Uchida N. 2012. Whole-brain mapping of direct inputs to midbrain dopamine neurons. Neuron. 74:858–873.

Weinberger NM. 2007. Associative representational plasticity in the auditory cortex: a synthesis of two disciplines. Learn Mem. 14:1–16.

Weissbourd B, Ren J, DeLoach KE, Guenthner CJ, Miyamichi K, Luo L. 2014. Presynaptic partners of dorsal raphe serotonergic and GABAergic neurons. Neuron. 83:645–662.

Wenk H, Bigl V, Meyer U. 1980. Cholinergic projections from magnocellular nuclei of the basal forebrain to cortical areas in rats. Brain Res. 2:295–316.

Whitehouse PJ, Hedreen JC, White CL, Price DL. 1983. Basal forebrain neurons in the dementia of Parkinson disease. Ann Neurol. 13:243–248.

Wilson FA, Rolls ET. 1990. Neuronal responses related to reinforcement in the primate basal forebrain. Brain Res. 509: 213–231.

Xu M, Chung S, Zhang S, Zhong P, Ma C, Chang WC, Weissbourd B, Sakai N, Luo L, Nishino S, et al. 2015. Basal forebrain circuit for sleep-wake control. Nat Neurosci. 18:1641–1647.

Yang X, Holmes MJ, Newton AT, Morgan VL, Landman BA. 2012. A comparison of distributional considerations with statistical analysis of resting state fMRI at 3T and 7T. Proc SPIE Int Soc Opt Eng. 8314: 831416.

Yarkoni T, Poldrack RA, Nichols TE, Van Essen DC, Wager TD. 2011. Large-scale automated synthesis of human functional neuroimaging data. Nat Methods. 8:665–670.

Yeo BT, Krienen FM, Sepulcre J, Sabuncu MR, Lashkari D, Hollinshead M, Roffman JL, Smoller JW, Zollei L, Polimeni JR, et al. 2011. The organization of the human cerebral cortex estimated by intrinsic functional connectivity. J Neurophysiol. 106:1125–1165.

Young WS 3rd, Alheid GF, Heimer L. 1984. The ventral pallidal projection to the mediodorsal thalamus: a study with fluorescent retrograde tracers and immunohistofluorescence. J Neurosci. 4:1626–1638.

Yuan R, Di X, Taylor PA, Gohel S, Tsai YH, Biswal BB. 2016. Functional topography of the thalamocortical system in human. Brain Struct Funct. 221:1971–1984.

Zaborszky L, Csordas A, Mosca K, Kim J, Gielow MR, Vadasz C, Nadasdy Z. 2015. Neurons in the basal forebrain project to the cortex in a complex topographic organization that reflects corticocortical connectivity patterns: an experimental study based on retrograde tracing and 3D reconstruction. Cereb Cortex. 25:118–137.

Zaborszky L, Cullinan WE, Braun A. 1991. Afferents to basal forebrain cholinergic projection neurons: an update. Adv Exp Med Biol. 295:43–100.

Zaborszky L, Duque A. 2003. Sleep-wake mechanisms and basal forebrain circuitry. Front Biosci. 8:d1146–d1169.

Zaborszky L, Hoemke L, Mohlberg H, Schleicher A, Amunts K, Zilles K. 2008. Stereotaxic probabilistic maps of the magnocellular cell groups in human basal forebrain. Neuroimage. 42:1127–1141.

Zaborszky L, Van Den Pol A, Gyengesi E. 2012. The basal forebrain cholinergic projection system in mice. In: The Mouse Nervous System. Amsterdam: Elsevier. p. 684–718.

Zhang S, Hu S, Fucito LM, Luo X, Mazure CM, Zaborszky L, Li CR. 2017. Resting-state functional connectivity of the basal nucleus of meynert in cigarette smokers: dependence level and gender differences. Nicotine Tob Res. 19:452–459.

Zhang D, Snyder AZ, Fox MD, Sansbury MW, Shimony JS, Raichle ME. 2008. Intrinsic functional relations between human cerebral cortex and thalamus. J Neurophysiol. 100:1740–1748.